

# CAPILLARY NUMBER AND FIBER ORIENTATION DEPENDENT WICKING PATTERN IN ELECTROSPUN MEMBRANES

**R Fischer<sup>1,2,3</sup>, P Boillat<sup>4,5</sup>, L Weidenbacher<sup>2,6</sup>, D Derome<sup>1</sup>, RM Rossi<sup>2</sup>, J Carmeliet<sup>3</sup>**

<sup>1</sup>*Empa, Laboratory for Multiscale Studies in Building Physics, Dübendorf, Switzerland*

<sup>2</sup>*Empa, Laboratory for Biomimetic Membranes and Textiles, St Gallen, Switzerland*

<sup>3</sup>*ETH Zürich, Chair of Building Physics, Zürich, Switzerland*

<sup>4</sup>*Paul Scherrer Institute, Laboratory for Neutron Scattering and Imaging, Villigen, Switzerland*

<sup>5</sup>*Paul Scherrer Institute, Electrochemistry Laboratory, Villigen, Switzerland*

<sup>6</sup>*ETH Zürich, Department of Health Sciences and Technology, Zürich, Switzerland*

robert.fischer@empa.ch

## ABSTRACT

Vertical wicking from an unlimited reservoir is investigated for electrospun ethylene vinyl alcohol membranes with varying fiber orientations. Neutron radiography is applied to create time-resolved maps of the moisture distribution during wicking. A transition at a critical capillary number from stable water front displacement to unsaturated capillary fingering is observed. While the wicking behavior appears to show little dependence on the fiber orientation during stable displacement, differences can be observed in terms of maximum height and finger shape during the later uptake phase with capillary fingering.

**Key Words:** CAPILLARY FINGERING, WICKING, ELECTROSPUN, FIBER ORIENTATION

## 1. INTRODUCTION

Electrospun membranes constitute a promising class of textile materials for biomedical and pharmaceutical applications, e.g. as artificial scaffold for muscle cells or for time-controlled drug delivery [1, 2], but also for moisture management in functional clothing. A profound understanding of the kinetics of the liquid transport in these fibrous mats is necessary for designing effective application.

Electrospun membranes are nonwoven meshes of continuous fibers with diameter usually ranging from a few nanometers to a few microns. Pores are formed as voids between the fibers during the deposition of the fibers. Capillary suction is created by subsequently wetting hydrophilic fibers and forming menisci. The minimization of surface energy drives the uptake of water into the membrane, known as capillary action.

The classic way of describing wicking in porous media from an unlimited reservoir is by the simple Washburn law. [3, 4]

$$h(t) = A\sqrt{t} \quad (1)$$

Where the wicking rate  $A$  is obtained by inserting the Laplace pressure of a tube into Poiseuille law. This approach requires a well-defined water front to be described by an advancing height  $h$ , which is not always readily identified experimentally. Also, the physical relevance of the parameters contributing to  $A$  has been questioned, e.g. Schoelkopf et al.[5] On the other side, Lenormand et al. [6] discussed a phase diagram of flow pattern in porous media depending on viscosity ratio and capillary number. The capillary number ( $Ca$ ) is a dimensionless number describing the relation of capillary to viscous forces, where  $\mu$  is the liquid viscosity,  $v$  the flow velocity and  $\gamma$  the surface tension.

$$Ca = \frac{\mu v}{\gamma} \quad (2)$$

Based on experimental observations, they distinguish between viscous fingering, stable displacement and capillary fingering. Any model that aims to describe wicking in fibrous materials needs to consider these flow pattern regimes and the ill definition of the waterfront when the displacement is not stable and fingering has happened.

Parada et al. [7] compiled an ample review of experimental methods to measure wicking properties in textiles. Neutron radiography stands out since it not only provides information of the liquid advance, but also on the amount of water per unit area.[8] This allows us to measure accurately wicking in textiles without relying on an ill-defined and un-sharp waterfront. In this paper, we investigate the vertical wicking behavior of water in electrospun ethylene vinyl alcohol (EVOH) with different fiber orientations from an unlimited reservoir.

## 2. METHODS

### 2.1 Production and preparation of electrospun membrane samples

A solution of 12% ethylene vinyl alcohol (EVOH, Soarnol, Nippon Gohsei, Japan) dissolved in hexafluoroisopropanol (Sigma Aldrich)(HFIP):water (3:1) was electrospun for 4h at 10ul/min, +16 -6kV electrode potentials from a distance of 25 cm, and collected on a 250x250mm aluminum foil wound around a rotating drum at rotation velocities ranging from 500 up to 2000rpm to induce different fiber orientation distributions.

Rectangular pieces of 30x60mm were cut from the homogeneous central part of the membrane using a razor blade and carefully removed from the aluminum foil. The 30mm sides of the membrane were sealed with an aluminum tape by folding the sticky side inwards and carefully flattening the attached tape. Small weights of soft lead were attached to the aluminum tape at one side to straighten the sample while placing it into the sample holder.

### 2.2 Neutron Radiography

Our experimental setup contains a reservoir that is connected to a bucket of deionized water. The sample is hanged into a frame, which is supported only by a balance to measure the change in mass. By remotely lifting the bucket, water flows into the reservoir submerging the base of the sample to instigate wicking. The setup is placed into the middle sample stage of the ICON beamline (SINQ, Paul Scherrer Institute, Villigen PSI, CH) for neutron radiography (Figure 1)

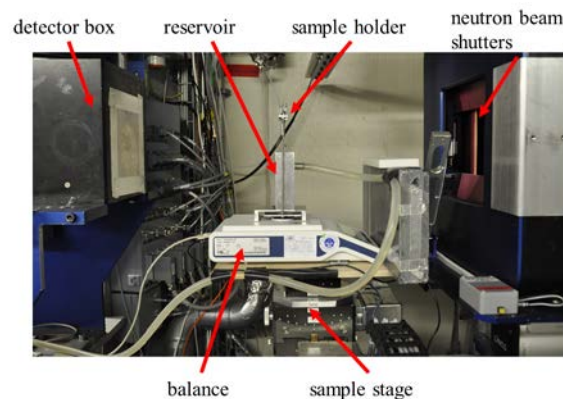


Figure 1: Neutron radiography setup. The sample stage is moved left during acquisition to place the sample as close to the detector as possible

Neutrons produced by the continuous spallation source are moderated by liquid deuterium to shift their spectrum to lower energies, pass an aperture system, penetrate the sample and finally hit a 20  $\mu\text{m}$  Gadox powder scintillator that converts the neutron beam intensity to visible light. Images of the scintillator are recorded by a CCD camera and stored as 16bit grayscale images with 2048 x 2048 pixels. The acquisition was optimized to 20s illumination time and 33  $\mu\text{m}$  pixel size.

Transmission of neutrons, as any particle penetrating matter, is based on their behavior at collisions. Cold neutrons, as used in our experiment, are generally readily scattered by the hydrogen nucleus, which makes them an excellent probe for moisture. The intensity of the neutron beam after transmitting the sample can be described by the Lambert-Beer law.

The neutron beam in our experiments is polychromatic but, for the sake of detecting moisture in the sample, the discussion of the Lambert-Beer-Law with a universal attenuation factor is sufficient. With the known attenuation factor of water  $\Sigma$ , the transmission length  $z$  can be determined and the mass of water  $w$  per pixel calculated. Thus, for our experiment, we obtain equations as follows:

$$I(x, y, t) = I_0(x, y) \cdot e^{-\Sigma z(x, y, t)} \quad (3)$$
$$w(x, y, t) = \rho_{H_2O} \cdot z(x, y, t)$$

The result is a time-resolved map of  $w$ , where moisture content has the unit  $kg\ m^{-2}$ . Several image-processing steps need to be followed to apply the Lambert-Beer law on the intensity images and obtain the moisture maps.

1. An outlier filter is applied to remove white spots from the raw images. This filter replaces pixel values deviating over a threshold from the median in its surrounding by the said median (radius = 2.5 pixel, threshold = 250).
2. The median of 5 images recorded at the beginning without beam is subtracted from the dataset as dark current.
3. A 3D-(2 space, 1 time)-Gaussian blur is applied on the dataset (sigma=0.75 pixel).
4. The median of the first 5 images (before releasing water) provides the pixel map of  $I_0$ .
5. Spurious scattering from the water reservoir is corrected by dividing the median intensity profile in a band of pixels not containing the sample from the full image.
6. The Lambert-Beer law (Equation 3) is applied pixel-wise on the dataset to obtain the time-resolved moisture maps  $w$  with  $\rho = 997kg\ m^{-3}$  and  $\Sigma = 470m^{-1}$  for the chosen scintillator-camera-combination.

To detect the moving liquid-air-interface in the membrane, additional processing steps are applied.

1. 2D-spatial median filter with radius 2.5 pixel.
2. The transition of pixels from dry to wet is detected as the maximum of the gradient of the low-pass filtered pixel value in temporal direction or if the value surpasses  $0.01\ kg\ m^{-2}$ .

### 3. RESULTS

Figure 2 shows examples of neutron radiography taken at two different times during the wicking experiment of an electro-spun membrane made at 500 rpm, with wicking occurring orthogonally to the fiber orientation. The moisture distribution (Figure 2 a) obtained at an early time step with a stable displaced waterfront and figure 2 (b) at a later stage after the occurrence of fingers. In the latter, two regions can be identified: a homogenously saturated area and a band of only partially saturated fingers of almost fractal shape. Figures 2 (c,d) display the segmentation of (a, b) in wet and dry areas. The interface evolution can be extracted from these segmented images. The average interface spreading velocity is calculated and displayed in Figure 3 (a). This velocity value is taken to determine the capillary number according to equation 2 with  $\mu = 1 \text{ mPa s}$  and  $\gamma = 72.6 \text{ mN m}^{-1}$ . The appearance of fingers causes consequently an increase of the interface perimeter. The relative perimeter by putting the perimeter at time  $t$  in relation to the perimeter at  $t \rightarrow 0$  describes the extent of finger formation. Comparing the capillary number ( $Ca$ ) to the relative perimeter reveals a common pattern: When the capillary number, i.e. the liquid velocity, drops below a critical capillary number of around  $\log(Ca_{crit}) \approx -6.7$  (Figure 3b), fingers start to appear and there is a steep increase of the relative perimeter. This transition is relatively smooth over a certain region of  $Ca$  until the fingers reach their full extent at  $\log(Ca) \approx -8$  (Figure 3b). While the overall dynamics (Figure 3) show only little difference between the sample parameter, the final height of the up-taken water varies with the sample parameters. (Figure 4)

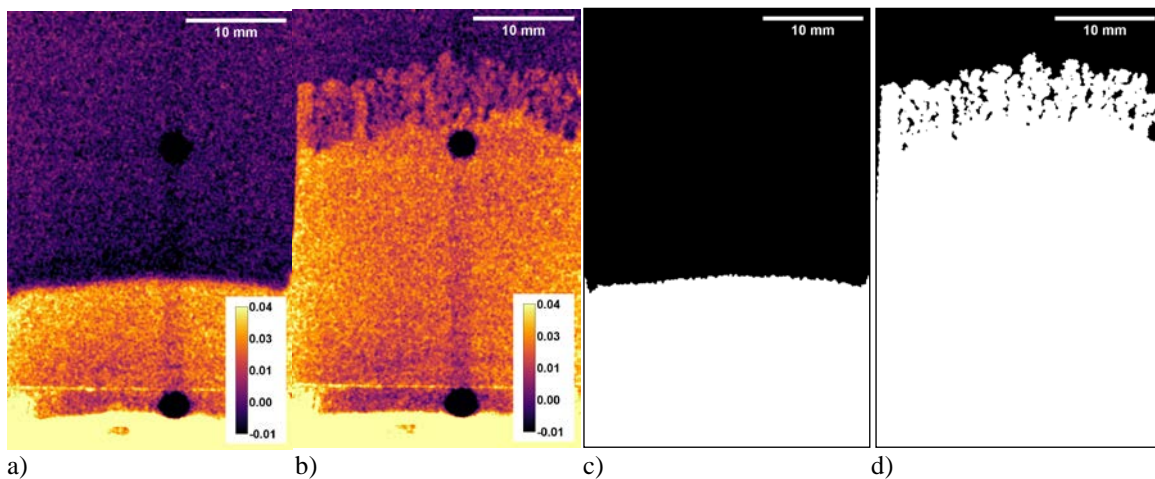
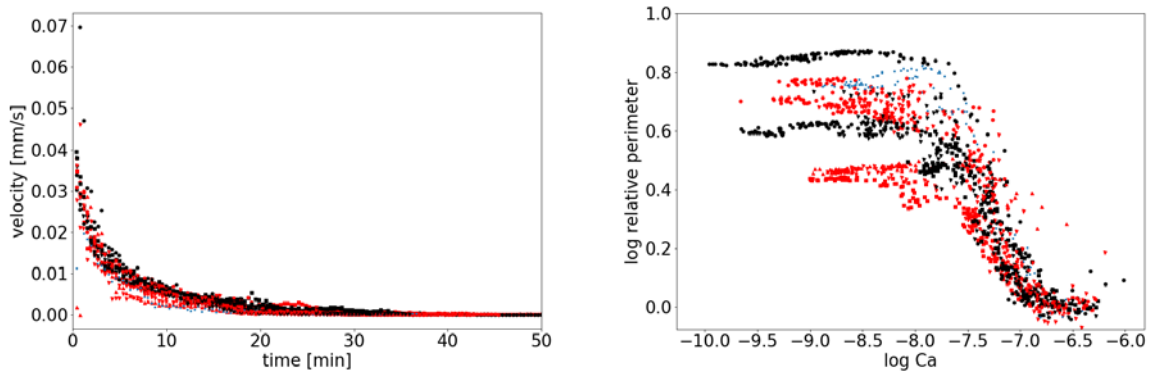
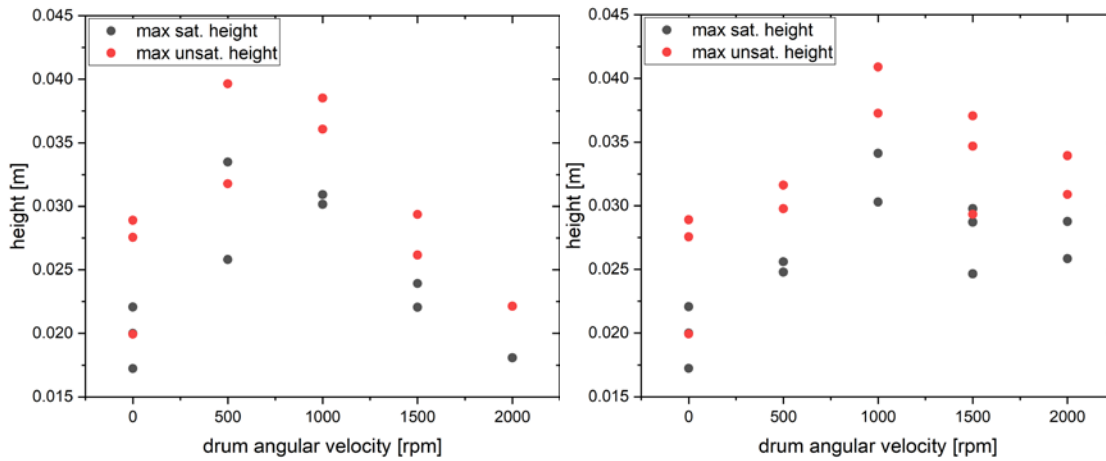


Figure 2: Moisture map at a)  $t = 4.5 \text{ min}$  and b)  $t = 35.9 \text{ min}$  with c,d) respective segmented images of the wetted area. The units of the color bar are  $\text{kg/m}^2$ , sample: 500rpm, wicking orthogonal to fiber orientation



a) b)  
 Figure 3: (a) Calculated spreading velocity of all samples, black (red): principal fiber orientation orthogonal (parallel) to wicking direction. (b) Increase of dry-wet-interface length vs. capillary number  $Ca$ , black (red): principal fiber orientation orthogonal (parallel) to wicking direction



a) b)  
 Figure 4: Maximum height of the (un)saturated waterfront in black (red) for wicking in the direction a) orthogonal and b) parallel to principal fiber orientation induced by variable rotation speed of the collector drum.

## 4. DISCUSSION

The experimental results are still undergoing analysis, but some observations can be drawn already. The critical Capillary number of  $\log(Ca_{crit}) \approx -6.7$  at the transition from stable displacement to fingering appears to be universal for this material. The fingering phenomenon can be identified as capillary fingering as already described by Lenormand et al. [6]. Inter-fibril pores are filled if capillary suction overcomes the flow resistance of viscous drag at the polymer-liquid interfaces. While the distance between advancing front and inlet grows, also the drag increases. When the stable front collapses at  $Ca_{crit}$ , liquid can only advance in randomly distributed percolating paths which provide sufficient capillary suction. This is due to the statistical distribution of pore sizes between the randomly deposited fibers. While the transition to fingering occurs in a narrow range of  $Ca$  for all samples (Figure 3b) and at a comparable time step (Figure 3a), the final height of both unsaturated and saturated liquid rise deviates among the sample parameters (Figure 4).

We interpret that, by varying the fiber orientation, we also change the network of flow paths and therefore the wicking behavior especially in the fingering regime. Naturally, wicking is enhanced in the parallel over the orthogonal fiber directions (1500 rpm, 2000 rpm in Figure 4). However, there seems to be an optimum of fiber orientation and cross-linking of horizontal

flow paths at 1000 rpm (Figure 4). All samples per parameter were taken from the same piece, and, despite careful preparation, batch dependencies like membrane thickness cannot be ruled out completely yet.

## 5. CONCLUSION

At this stage of the investigation, the observed behavior might be typical for fibrous porous media and the flow regimes of stable displacement and capillary fingering should be considered also in different systems like textile yarns. There seems to be a critical capillary number, which denotes the transition between flow regimes. While the wicking behavior appears to show little dependence on the fiber orientation during stable displacement, differences can be observed in terms of maximum height and finger shape during the later uptake phase with capillary fingering.

## Acknowledgments

The authors thank Stefan Carl for the support during designing and manufacturing the experimental setup. R Fischer thanks J Allegrini, F Qin, J Shah and D Strebel for the help during the measurements. Our measurements were performed at the ICON: Imaging with Cold Neutrons beamline at the Swiss Spallation Neutron Source (SINQ) of the Paul Scherrer Institute (PSI) in Villigen, Switzerland.

## References

1. Stankus, J.J., et al., *Fabrication of cell microintegrated blood vessel constructs through electrohydrodynamic atomization*. *Biomaterials*, 2007. **28**(17): p. 2738-46.
2. Weidenbacher, L., et al., *Electrospraying of microfluidic encapsulated cells for the fabrication of cell-laden electrospun hybrid tissue constructs*. *Acta Biomater*, 2017. **64**: p. 137-147.
3. Washburn, E.W., *The Dynamics of Capillary Flow*. *Physical Review*, 1921. **17**(3): p. 273-283.
4. Kissa, E., *Wetting and wicking*. *Textile Research Journal*, 1996. **66**(10): p. 660-668.
5. Schoelkopf, J., et al., *Practical observation of deviation from Lucas-Washburn scaling in porous media*. *Colloids and Surfaces A: Physicochemical and Engineering Aspects*, 2002(206): p. 445-454.
6. Lenormand, R., E. Touboul, and C. Zarcone, *Numerical models and experiments on immiscible displacements in porous media*. *Journal of Fluid Mechanics*, 1988. **189**(-1).
7. Parada, M., et al., *A review on advanced imaging technologies for the quantification of wicking in textiles*. *Textile Research Journal*, 2017. **87**(1): p. 110-132.
8. Parada, M., et al., *Dynamic Wicking Process in Textiles*. *Transport in Porous Media*, 2017. **119**(3): p. 611-632.